Radiation wavelength dependence of clearing channel characteristics in a trail behind supersonic civil aircraft

A.N. Kucherov

N.E. Zhukovskii Central Institute for Aerohydrodynamics, Moscow

Received April 29, 2005

Estimations and calculations of clearing (vaporization) channel characteristics in the trail behind advanced civil supersonic aircraft are made for the maximal optical thickness cross section. The infrared wavelength range of the laser vaporizing water aerosol is considered.

Introduction

The light absorption and scattering by small aerosol particles[1–3] play an essential role in ecological problems of remote sensing of the air transport emission,[4–6] in particular, in the problem of a clearing channel formation at a condensation trail.[7] Subsonic airbuses, which are principal emission sources, cruise at altitudes of 10–13 km. Projected civil supersonic aircrafts of the 2nd generation – Russian SPS-2 (Ref. 8) and American HSCT (High Speed Civil Transport)[9] – are planned to fly at altitudes about 18 km. At such altitudes, clouds and the condensation trail (contrail) mainly consist of ice. Crystalline ice particles of water aerosol in clouds, mists, and contrail can be united into 3 groups: 1) spheres (volumetrical particles), 2) cylinders and needles, and 3) plates and disks.[10,11] Particle sizes in a contrail can reach 10 μm (by the order of magnitude).[12] The atmosphere is the most transparent for IR laser radiation at $\lambda = 2.91$, 3.80, 5.058, and 10.6 μm.[13–15] In this paper, optical characteristics of the clearing (vaporization) channel at the trail behind a civil supersonic aircraft are considered. The channel needs for examination of the exhaust jet central part with maximal concentration of contaminants, i.e., nitric oxides, sulphides and chlorides. Consider spherical particles of mono- and polydisperse aerosol.

1. Optical parameters of ice spheres

Heating, sublimation, melting, and vaporization of particles of three principal shapes have been investigated in Ref. 11 at $\lambda = 10.6$ μm. The complex refraction coefficient for water and ice in IR $m = n_{i,w} + i\kappa_{i,w}$ ($n_{i,w}$ is the real refraction index, $\kappa_{i,w}$ is the absorption index, i corresponds to ice and w to water) is given in Refs. 16–18.

The Mie theory[3,19] provides solutions inside and outside a particle and allows one to calculate factors and cross sections of radiation absorption, scattering, and extinction at a single particle. The heat emission intensity q of the absorbed radiant energy W_{abs} is a function of the medium-volume absorption coefficient α_{abs}, cross section σ_{abs}, and efficiency factor of radiation absorption by a particle Q_{abs} (Ref. 3):

$$q = \frac{W_{abs}}{V} = \frac{\int \alpha_{i,w} I \mathrm{d}V}{V} = \alpha_{abs} I_0;$$

$$Q_{abs} = \frac{W_{abs}}{SI_0} = \frac{\alpha_{abs} V}{S} = \frac{\sigma_{abs}}{S}, \qquad (1)$$

where V is the particle volume ($V = 4\pi a^3/3$ for sphere of radius a); $\alpha_{i,w} = 4\pi\kappa_{i,w}/\lambda$ is the radiation absorption coefficient; I_0 is the incident radiation intensity; $S = \pi a^2$ is the square of the particle section by a plane normal to the incident beam axis.

In the case of some nonabsorbing medium, the energy extinction $W_{ext} = W_{abs} + W_{sca}$, where W_{abs} is absorbed (in the volume V per unit time) and W_{sca} is the scattered energy. Therefore, $\sigma_{ext} = \sigma_{abs} + \sigma_{sca}$. Factors, sections, and absorption and extinction coefficients ($Q_{sca} = \sigma_{sca}/\pi a^2$; $Q_{ext} = \sigma_{ext}/\pi a^2$; $\alpha_{sca} = 3Q_{sca}/4a$; $\alpha_{ext} = 3Q_{ext}/4a$) are calculated by well-known formulae and algorithms.[1–3] Optical parameters of a particle depend on the radius a, radiation wavelength λ, as well as the matter of the particle and surrounding medium (i.e., complex refraction index $m = n + i\kappa$). Set $n = 1$ and $\kappa = 0$ for the air outside a particle. Specific to mass unit coefficients of absorption, scattering, and extinction are $b_{abs,sca,ext} = \alpha_{abs,sca,ext}/\rho_{ice}$, where ρ_{ice} is the density of particle matter (here $\rho_{ice} = 900$ kg/m^3 is the ice density). Coefficients of absorption, scattering, and extinction for aerosol are defined as a multiplication

$$\beta_{abs,sca,ext} = b_{abs,sca,ext}\, \rho_{i,w},$$

where $\rho_{i,w}$ (kg/m^3) is the ice or water content of aerosol, i.e., the mass of a condensate (ice or water) per unit volume.

In reality, aerosol is polydisperse and its particles differ in size. A typical a-size distribution function

0235-6880/05/10 783-06 $02.00

$f(a)$ for aerosol particles in clouds is the gamma-distribution with two parameters: modal radius a_{mod} and μ, e.g. Khrgian–Mazin distribution, $\mu = 2$ (Ref. 10). Specific coefficients of spheres can be size-averaged according to the following equations[20,21]:

$$b = \frac{\alpha}{\rho_{\text{i,w}}} = \frac{\pi N_d \int_0^\infty a^2 Q(a) f(a) \mathrm{d}a}{\frac{4}{3}\pi N_d \rho_{\text{ice}} \int_0^\infty a^3 f(a) \mathrm{d}a};$$

$$f(a) = \frac{\mu^{\mu+1}}{\Gamma(\mu+1)} \frac{a^\mu}{a_{\text{mod}}^{\mu+1}} \mathrm{e}^{-\mu \frac{a}{a_{\text{mod}}}}; \quad \int_0^\infty f(a)\mathrm{d}a = 1. \qquad (2)$$

Here $\Gamma(\mu)$ is the gamma-function and N_d is the number of particles per unit volume.

Figure 1 shows the specific extinction coefficient $b_{\text{ext}} = \alpha_{\text{ext}}/\rho_{\text{ice}}$ (m^2/kg) of mono- (Fig. 1*a*) and polydisperse aerosol (Fig. 1*b*) as a function of the radius a at different wavelengths. Figure 1*b* presents specific coefficients for polydisperse aerosol of spheres as functions of the modal radius a_{mod}. Accounting for size-distribution of particles results in decreasing of the maximum and its displacement to the region of small radii.

Table 1 presents the dependence of the absorption factor Q_{abs} and the extinction factor Q_{ext} on λ in IR range (1–10 μm), as well as of specific coefficients of absorption (b_{abs}) and extinction (b_{ext}) at a single particle (sphere radii are 0.1, 1.5, and 10 μm). At $\lambda = 1.06$ μm, b_{abs} and b_{ext} are 10^3–10^5 times greater than the specific absorption coefficient for ice $b_{\text{i}} = \alpha_{\text{i}}/\rho_{\text{ice}}$. The ice-content $\rho_{\text{i}} \sim 10^{-5}$ kg/m^3 in the cross section of the maximal optical thickness is characteristic for the SPS-2 trail, studied in the paper (see section 2). Characteristic (exponential) lengths of absorption $L_{\text{abs}} = 1/(\rho_{\text{i}} b_{\text{abs}})$ and attenuation $L_{\text{ext}} = 1/(\rho_{\text{i}} b_{\text{ext}})$ are the following: at $\lambda = 10.6$ μm $L_{\text{abs}} = 1370$, 1251, and 1538 m and $L_{\text{ext}} = 1376$, 1080, and 552.4 m (for $a = 0.1$, 1.5, and 10 μm, respectively); at $\lambda = 1.06$ μm, $L_{\text{abs}} = 3.33 \cdot 10^6$; $2.0 \cdot 10^6$, and $2.24 \cdot 10^6$ m and $L_{\text{ext}} = 1080$, $5.676 \cdot 10^5$, and 526.8 m. At $\lambda \le 2$ μm, the energy scattering considerably exceeds its absorption. Translucence due to evaporation is ineffective since the radiation intensity decreases due to scattering along the beam earlier than aerosol is evaporated by the absorbed energy.

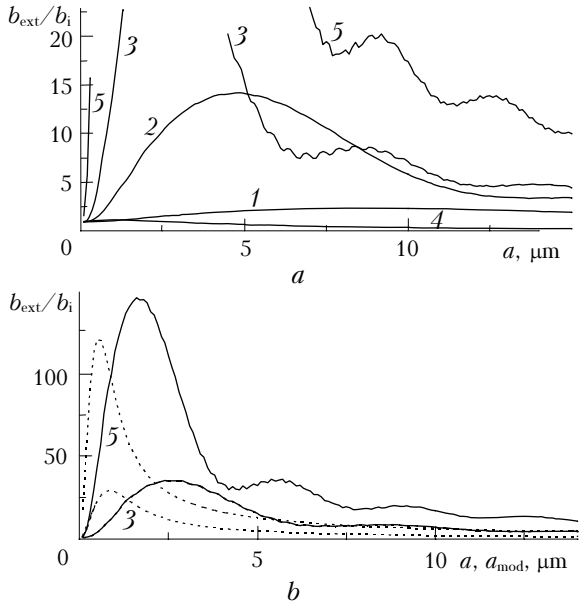

Fig. 1. A sphere. Extinction coefficient $b_{\text{ext}}/b_{\text{i}} = \alpha_{\text{ext}}/\alpha_{\text{i}}$ in accordance with the particle radius: monodisperse aerosol (*a*); $\lambda = 10.6$ μm (*1*), 5.058 (*2*), 3.80 (*3*), 2.91 (*4*), and 2.0 μm (*5*); dashed lines correspond to polydisperse aerosol (*b*).

Table 1. Absorption factor Q_{abs} and extinction factor Q_{ext}, specific coefficients of absorption b_{abs} and extinction b_{ext} as functions of wavelength λ and radius a (μm) of an ice aerosol particle. Monodisperse aerosol

Wavelength λ, μm	10.6	5.058	3.80	2.91	2.0	1.06
n_{i}	1.195	1.243	1.356	1.131	1.291	1.301
κ_{i}	0.0602	0.0131	0.0082	0.12	0.00161	$2.4 \cdot 10^{-6}$
Q_{abs}, $a = 0.1$	$8.719 \cdot 10^{-3}$	$3.879 \cdot 10^{-3}$	$3.03 \cdot 10^{-3}$	0.06593	$1.20 \cdot 10^{-3}$	$3.6 \cdot 10^{-6}$
1.5	0.1439	0.0778	0.0770	0.7706	0.0307	$9.08 \cdot 10^{-5}$
10	0.780	0.496	0.468	1.106	0.191	$5.36 \cdot 10^{-4}$
Q_{ext}, $a = 0.1$	$8.719 \cdot 10^{-3}$	$3.89 \cdot 10^{-3}$	$3.12 \cdot 10^{-3}$	0.0660	$2.05 \cdot 10^{-3}$	0.01107
1.5	0.1667	0.3696	1.407	1.108	2.896	3.172
10	2.282	2.514	2.566	2.166	2.350	2.278
b_{i}, m^2/kg	79.3	36.2	30.1	576	11.2	0.0316
b_{abs}, $a = 0.1$	72.66	32.36	25.2	549.5	10.0	0.030
1.5	79.9	43.2	42.7	428.5	17.0	0.050
10	65.0	43.3	39.0	92.2	15.9	0.0446
b_{ext}, $a = 0.1$	72.66	32.49	26.0	550.03	17.1	92.2
1.5	92.62	205.6	781.1	615.7	1609	1762
10	181.0	209.6	213.6	180.6	195.8	189.8

2. Exhaust jet evolution

Consider evolution of the exhaust jet of a supersonic civil aircraft SPS-2 of the 2nd generation. Take the standard atmospheric model.[22] Describe the diffuse mixing with the atmosphere by the Prandtl boundary equations within the Kovazhnyi–Sekundov one-parameter turbulence model.[21,23,24] An isobaric stationary axially-symmetric exhaust jet is described by a set of equations of conservation of mass, momentum, and energy; vapor diffusion equation; as well as equations for coefficients of turbulent kinematic viscosity ν and number density N_d of carbon condensation centers[21,25]:

$$\rho u\frac{\partial \nu}{\partial x}+\rho v\frac{\partial \nu}{\partial r}=\frac{2}{r}\frac{\partial}{\partial r}\left\{r\rho\nu\frac{\partial \nu}{\partial r}\right\}+A_T\rho\nu\left|\frac{\partial u}{\partial r}\right|, \qquad (3)$$

$$\left(\rho u\frac{\partial}{\partial x}+\rho v\frac{\partial}{\partial r}\right)\frac{N_d}{\rho}=$$

$$=\frac{1}{r}\frac{\partial}{\partial r}\left(r\rho D\frac{\partial}{\partial r}\frac{N_d}{\rho}\right)-2\sqrt{2}\pi V_T N_d^2 a_{mod}^2 B_2\eta_{cg}. \qquad (4)$$

Here ρ is the gas mixture density; u and v are the velocity components; A_T is a constant; D is the diffusion coefficients for particles in the gas mixture

$$B_k=\int_0^\infty\left(\frac{a}{a_{mod}}\right)^k f\,da=\frac{(\mu+1)(\mu+2)\ldots(\mu+k)}{\mu^k}$$

is constant for polydisperse aerosol (k and μ are integer, $\mu=2$ in the Khrgian–Mazin distribution, $B_2=3$) and $B_2=1$ for monodisperse aerosol; $V_T=C_{VT}\sqrt{(\nu u(r=0)/r_j)}$ is the rate of turbulent pulsation; C_{VT} is a constant; r_j is the jet radius; η_{cg} is the coefficient of particle coagulation (further $\eta_{cg}=0.5,\ 1$); the condensate concentration $\rho_i=\rho-\rho_{vs}$, where $\rho_{vs}(T, p)$ is the concentration of vapor saturated above ice at the temperature T and pressure p. Sizes of monodisperse aerosol particles a_w and modal (most probable) sizes of polydisperse aerosol particles a_{mod} can be found as

$$\rho_i=\frac{4}{3}\pi\rho_{ice}N_d\int_0^\infty a^3 f\,da\equiv\frac{4}{3}\pi\rho_{ice}N_d a_w^3,$$

$$a_w=a_{mod}(B_3)^{1/3}. \qquad (5)$$

For numerical solution of the problem, an implicit finite-difference model is used.[26] The SPS-2 fly parameters are the following: the altitude $h=18$ km, pressure $p_\infty=0.0756$ N/m^2, atmosphere temperature $T_\infty=216.66$ K, speed $u_\infty=590$ m/s. Let relative mass concentration of vapor be $Y_\infty=0$. Parameters at the jet engine nozzle are the following: the exhaust gas temperature $T_a=407$ K, velocity $u_a=1000$ m/s, concentration of gas $Y_a=0.0157$ and of carbonic acid $Y_{aCO_2}=0.0480$, and nozzle radius $r_a=0.87$ m. Let us consider two variants of the turbulent mixing: I) $A_T=0.2$, $C_{VT}=1$, $\eta_{cg}=0.5$ and II) $A_T=0.4$, $C_{VT}=5$, $\eta_{cg}=1$. Take the initial numerical density of carbon condensation centers $N_{da}=10^{13}$ m^{-3} (variant I), 10^{10} m^{-3} (variant II), and 10^7 m^{-3} (variant IIa).

The initial part of the exhaust jet, where the velocity, temperature, concentration of vapor and other impurities are constant and uniform, terminates at the distance $x\geq 10r_a$. In the next transient part of the jet, the excess velocity $u_1=u-u_\infty$, temperature $T_1=T-T_\infty$, and vapor concentration $Y_1=Y-Y_\infty$ decrease rapidly. Coefficients of kinematic viscosity first rapidly rise up to some $x_{\nu m}$ value (49.6 m for variant I and 26.4 m for variant II), and then slowly decrease. Condensation begins in cold and distant from the jet axis regions of trail. In the cross section $x_*=344$ (I) and 175.2 m (II), aerosol closes down the axis; in $x_{\tau m}=466$ (I) and 237 m (II), the transversal optical thickness $\tau(x)=\int\beta_{ext}(r,\ x=\text{const})dr$ reaches its maximum $\tau_m=0.00217$ (I) and 0.0608 (II). These values correspond to monodisperse aerosol ($\lambda=3.80$ μm).

In the cross section $x_{Y_m}=568$ (I) and 287 m (II), the mass concentration of the condensate Y_i reaches its maximum $Y_{im}=9.11\cdot10^{-5}$ (I) and $9.11\cdot10^{-5}$ (II) while the condensate density maximum $\rho_{im}=1.06\cdot10^{-5}$ kg/m^3 falls at the cross section $x_{am}=720$ (I) and 364 m (II); here particle sizes reach maximal values $a_{max}=0.1725$ μm (I) and 1.689 μm (II).

Figure 2 shows distribution of particle radii $a(x)$ and optical thickness $\tau(x)$ along the jet axis for variants I and II for monodisperse aerosol at $\lambda=3.80$ μm.

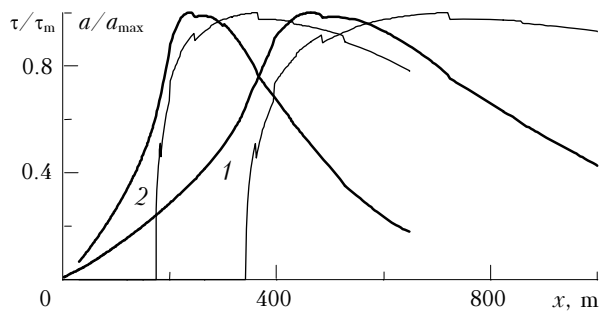

Fig. 2. Particle radii $a(r=0,\ x)$ (thin curves) and the contrail optical thickness $\tau(x)$ (bold curves) as functions of the distance x from the nozzle of jet engines of SPS-2. Variant I (curves *1*): $\eta_{cg}=0.5$, $A_T=0.2$, $C_{VT}=1$, $N_{da}=10^{13}$ m^{-3}; $\tau_m=0.00217$ ($x_{\tau m}=466$ m), $a_{max}=0.173$ μm ($x_{am}=720$ m). Variant II (curves *2*): $\eta_{cg}=1$, $A_T=0.4$, $C_{VT}=5$, $N_{da}=10^{10}$ m^{-3}; $\tau_m=0.0608$ ($x_{\tau m}=237$ m), $a_{max}=1.69$ μm ($x_{am}=364$ m). Monodisperse aerosol.

If to take $N_{da}=10^7$ m^{-3} in variant II (IIa), then maximal size of particles $a_{max}=16.255$ μm ($x_{am}=364$ m). Maximal optical thickness $\tau_m=0.00123$ ($x_{\tau m}=180.6$ m) and 0.00324 ($x_{\tau m}=180.6$ m) at $\lambda=3.80$ and 10.6 μm.

For variant I, Fig. 3 shows transversal to the jet axis distribution of the optical thickness $\tau(z)$ (where $z=r-r_j$ is the coordinate along the laser beam

propagation direction) in the cross section of its maximum at $\lambda = 10.6$, 5.058, 3.80, and 2.91 μm ($\tau_m = 0.0055$, 0.00249, 0.00217, and 0.0420).

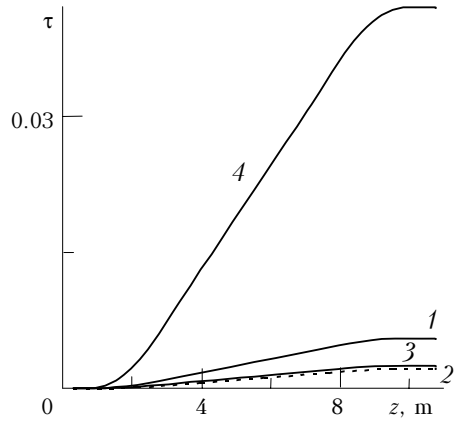

Fig. 3. Transversal distribution of the contrail optical thickness in the maximum cross section: $\lambda = 10.6$ μm ($x_{\tau m} = 462$ m) (*1*); 5.058 (458) (*2*); 3.80 (466) (*3*); and 2.91 μm (458 m) (*4*).

3. Clearing channel

Formulation of the problem of a clearing channel formation by a laser beam is the following.[20] A beam, scanning the exhaust jet with the flying speed u_∞ (nonmoving relative to the atmosphere), is directed transversely the jet (along the axis $z = r - r_j$) in the cross section of maximal optical thickness. In the water content approximation, the laser beam propagation is described by the following equations in the beam radius scale, which is an order of magnitude less than the jet radius r_j and the contrail one r_c ($r_0 \ll r_c \sim r_j$):

$$-2iF\frac{\partial E}{\partial z} + \nabla_\perp^2 E = F[-2FN_T\rho_1 + i(N_\alpha + wN_b)]E; \quad (6)$$

$$E|_{z=0} = e^{-(x^2+y^2)/2}; \; E|_{x,y\to\pm\infty} \to 0;$$

$$\frac{\partial w}{\partial t} + V(z)\frac{\partial w}{\partial x} = -wIN_v; \quad (7)$$

$$w|_{t=0;\,x\to-\infty} = w_0(z);$$

$$N_v = \frac{b_{abs}I_0\eta r_0}{H_{i,w}V_0}; \quad (8)$$

$$\left(\frac{\partial}{\partial t} + V(z)\frac{\partial}{\partial x}\right)\rho_1 = -I[N_{rel} + w];$$

$$\rho_1|_{t=0;\,x\to-\infty} = 0; \qquad N_{rel} = \frac{\alpha_{gas}}{\alpha_*}.$$

The x-coordinate (in the r_0-beam scale) is still directed along the transversal component of the beam and medium relative velocity $V_0V(z)$, i.e., along the jet axis. Here E is the wave function of electromagnetic field and $I = EE^*$ is the radiation intensity. All the quantities are dimensionless. The field function E is related to $\sqrt{I_0}$, transversal coordinates x and y – to the beam radius r_0, the beam-directed coordinate z – to the path length $L \sim 2r_c$, and the gas mixture density ρ is related to its unperturbed axial value $\rho_0 = \rho(r = 0, x_{\tau m})$. The similarity parameters are the following: $F = 2\pi r_0^2 n_0/\lambda L$ is the Fresnel number; r_0 is the beam radius, L is the characteristic path length, $N_b = b_{ext}\rho_{i0}L$ is the radiation attenuation by aerosol particles; $\rho_{i0} = \rho_i(x_{\tau m}, 0)$ is the characteristic water (ice) content of aerosol; $N_\alpha = \alpha_{gas}L$, is the parameter of radiation attenuation by a gas mixture, α_{gas} is the factor of radiation absorption by a gas mixture; $N_T = Q(r_0/L)^2(n_0 - 1)/n_0$ is the thermal blooming, n_0 is the refraction index of unperturbed gas; $Q = (\alpha_* I_0 r_0)/(\rho_0 h_0 V_0)$ is the scale of gas density perturbation, connected with the relative density perturbation $\Delta\rho/\rho_0$ through the relation $\Delta\rho/\rho_0 = Q\rho_1$, where ρ_1 is the dimensionless function of the gas density perturbation; $I_0 = P_0/\pi r_0^2$ is the characteristic radiation intensity, where P_0 is the initial beam power; $\alpha_* = (1 - \eta)\beta_{abs}$ is the effective coefficient of radiation absorption by aerosol; η is the evaporation efficiency of an individual particle, $\beta_{abs} = b_{abs}r_{i0}$ is the coefficient of radiation absorption by aerosol, $h_0 = C_pT_0$, T_0 are the enthalpy and the temperature of unperturbed gas, C_p is the heat capacity at a constant pressure; $V_0 = u(r = 0, x_{\tau m}) - u_\infty$ is the excess jet velocity on the axis (the characteristic velocity of the beam transversal airflow); $N_v = b_{abs}I_0\eta t_0/H_{i,w}$ is the vaporization (clearing) parameter, where $H_{i,w}$ is the specific heat of water evaporation or ice sublimation, $t_0 = r_0/V_0$ is the characteristic aerodynamic time; N_{rel} is the ratio of gas-absorbed energy to aerosol-absorbed energy; $w_0(z)$ is the initial distribution of the dimensionless ice content function $w = \rho_i/\rho_{i0}$.

The initial wave front is plane. The initial transversal intensity distribution is Gaussian. The ice content function w is described by the transfer equation (7) and the gas heating – by Eq. (8). The speed V is locally independent (in the scale of the beam radius r_0) of x and y in view of $r_0 \ll L$. The beam-lengthwise speed component is bound to occur when scanning beam relative to atmosphere and, in first approximation, has no effect on the beam.

Consider the particular examples. The SPS-2 aircraft cruises at an altitude of 18 km (variant I of turbulent mixing in the exhaust jet). The trail in the cross section of the maximal optical thickness $x_{\tau m} \approx 460$ m, where $r_c = 4.51$ m. Take $r_0 = 0.05$ m, $L = 10.4$ m, $I_0 = 1.27 \cdot 10^4$ kW/m^2.

Transversal to beam distributions of the jet ice content function $\rho_i(x)$ and the optical thickness $\tau(x)$ are shown in Fig. 4 in different moments of time. Formation of a region of values of ice content function and optical thickness, reduced to an order of magnitude, i.e., clearing channel, is demonstrated.

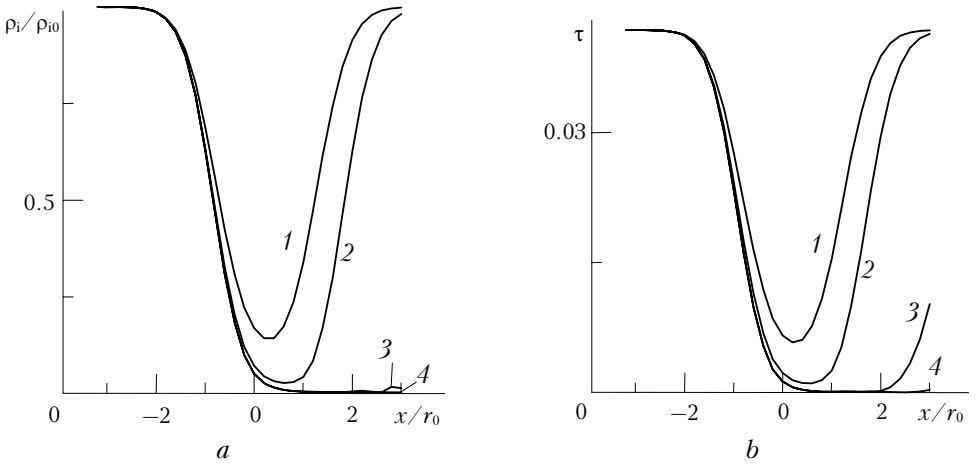

Fig. 4. Dynamics of the clearing channel formation: transversal to laser beam distributions of the ice content function at the jet axis $w(x) = \rho_i(x)/\rho_{i0}$ (*a*) and transversal distributions of the optical thickness $\tau(x)$ in the channel (*b*); $\lambda = 2.91$ μm; $t/t_0 = 0.5$ (*1*), 1 (*2*), 3 (*3*), 5 (*4*); SPS-2 aircraft: $V_0 = u(r = 0, x_{\tau m}) - u_\infty = 18$ m/s, $r_0 = 0.05$ m, $t_0 = r_0/V_0 = 2.78 \cdot 10^{-3}$ s, $\rho_{i0} = 1.01 \cdot 10^{-5}$ kg/m^3.

Table 2. Similarity parameters and characteristics of a medium (trail) and a beam into the clearing channel: extinction parameter N_b, clearing parameter N_v, initial ice content $\rho_{i0} = \rho_i(z = L/2)$; minimal relative ice content $\rho_{i,min}(L/2)/\rho_{i0}$ in the jet axis into the channel; initial optical half-thickness $\tau_{m2} = \tau(L/2)$, minimal optical half-thickness into the channel $\tau_{min}(L/2)$; fraction change in optical half-thickness $\Delta\tau(L/2)/\tau_{m2}$; initial optical thickness $\tau_m = \tau(L)$, minimal optical thickness into the channel $\tau_{min}(L)$; fraction change in optical half-thickness $\Delta\tau(L)/\tau_{m2}$ (time $t = 5t_0$, coordinates $x = 0 = y$)

Wavelength λ, μm	10.6	5.058	3.80	2.91
Variant I				
$N_b = b_{ext}\rho_{i0}L$, poly-,	0.00871	–	–	0.0632
monodisperse aerosol	0.00776	0.00348	0.003	0.0586
$N_v = \beta_{abs}I_0\eta t_0/H_i$, poly-,	0.471	–	–	3.420
monodisperse aerosol	0.456	0.202	0.162	3.440
$\rho_{i0} = \rho_i(z = L/2)$, kg/m^3, poly-,	$1.01 \cdot 10^{-5}$	–	–	$1.01 \cdot 10^{-5}$
monodisperse aerosol	$1.02 \cdot 10^{-5}$	$1.01 \cdot 10^{-5}$	$1.03 \cdot 10^{-5}$	$1.02 \cdot 10^{-5}$
$\rho_{i,min}(L/2)/\rho_{i0}$, poly-,	0.663	–	–	0.0523
monodisperse aerosol	0.672	0.838	0.868	0.0513
$\tau_{m2} = \tau(L/2)$, poly-,	0.00324	–	–	0.0236
monodisperse aerosol	0.00275	0.00130	$1.12 \cdot 10^{-3}$	0.0218
$\tau_{min}(L/2)$, poly-,	0.00194	–	–	0.000740
monodisperse aerosol	0.00174	0.00104	$9.4 \cdot 10^{-4}$	0.000665
$\Delta\tau(L/2)/\tau_{m2}$, poly-,	0.402	–	–	0.969
monodisperse aerosol	0.367	0.20	0.042	0.969
$\tau_m = \tau(L)$, poly-,	0.00625	–	–	0.0453
monodisperse aerosol	0.00549	0.00249	0.002152	0.042
$\tau_{min}(L)$, poly-,	0.00372	–	–	0.001426
monodisperse aerosol	0.00333	0.0020	0.001801	0.001299
$\Delta\tau(L)/\tau_m$, poly-,	0.404	–	–	0.969
monodisperse aerosol	0.393	0.20	0.163	0.970
Variant II, monodisperse aerosol				
N_b	0.010	0.0235	0.0861	0.0722
N_v	0.505	0.279	0.272	3.643
$\rho_{i0} = \rho_i(z = L/2)$, kg/m^3	$1.03 \cdot 10^{-5}$	$1.05 \cdot 10^{-5}$	$1.04 \cdot 10^{-5}$	$1.02 \cdot 10^{-5}$
$\rho_{i,min}(L/2)/\rho_{i0}$	0.644	0.786	0.80	0.0435
$\tau_{m2} = \tau(L/2)$	0.00367	0.00850	0.0314	0.02687
$\tau_{min}(L/2)$	0.00212	0.00268	0.0234	0.00068
$\Delta\tau(L/2)/\tau_{m2}$	0.423	0.261	0.254	0.747
$\tau_m = \tau(L)$	0.00704	0.0163	0.0603	0.05162
$\tau_{min}(L)$	0.00406	0.0121	0.0452	0.00131
$\Delta\tau(L)/\tau_m$	0.423	0.260	0.249	0.746

Maximal values of transversal optical thickness τ_m and reduction of optical thickness into the channel in the jet axis at $z = L/2$ and at the end of the beam propagation path at $z = L$ for a contrail (a trail behind the SPS-2) are presented in Table 2 for two variants of the turbulent mixing at four radiation wavelengths for mono- and polydisperse aerosol.

Note, that the diffraction broadening and heat blooming of a beam are negligible for the considered examples: $F \gg 1$ and $N_T \ll 1$. The analysis of results shows the following. The clearing is the most effective at $\lambda = 2.91$ μm, here the parameter of clearing N_v takes its highest values, a relative decrease in jet optical half-thickness $\Delta\tau(L/2)/\tau_{m2}$ and thickness $\Delta\tau(L)/\tau_m$ is maximal. The main cause is in high values of the index $\kappa_i = 0.12$ and absorption coefficient $b_i = 576$ m^2/kg as compared to other wavelengths. Specific coefficients of scattering and extinction do not exceed in the order of magnitude the corresponding values of specific coefficients of absorption. The wavelength ($\lambda = 10.6$ μm) is one more cause affecting the efficiency of the clearing process.

The turbulence amplification in the exhaust jet (change from variant I to variant II) results in an order of magnitude increase in particle maximal sizes (two orders of magnitude in variant IIa).

Accounting for aerosol polydispersion in the investigated trail behind the SPS-2 does not lead to a strong change in the optical thickness τ_m and values of their diminishing $\Delta\tau/\tau_m$ in the clearing channel. A similar result was obtained for IL-86 and IL-96 subsonic airbuses.[21]

Conclusion

The study of the influence of IR laser radiation wavelength on clearing of an exhaust jet (contrail) has shown the scattering to exceed the absorption and to interfere water evaporation in the region of short waves ($\lambda < 2$ μm).

Among the wavelengths investigated within the clearing channel formation problem (10.6, 5.058, 3.80, and 2.91 μm), falling into atmospheric transparency windows, $\lambda = 2.91$ and 10.6 μm are the most suitable for the clearing process. Aerosol polydispersion does not affect significantly the process.

Acknowledgments

This work was financially supported by ISTC (Grant No. 2249) and the State Program for Support of Leading Scientific Schools NSh-1984.2003.

References

1. H.C. Van de Hulst, *Light Scattering by Small Particles* (Wiley, J., & Sons, Inc., New York, 1957).
2. D. Deirmendjian, *Electromagnetic Scattering on Spherical Polydispersions* (Elsevier, New York, 1969).
3. C.F. Bohren and D.R. Huffman, *Absorption and Scattering of Light by Small Particles* (Wiley, New York, 1983).
4. *Proceedings of International Colloquium on Impact of Aircraft Emissions upon the Atmosphere* (Paris, 1996), Vol. I, pp. 1–378; Vol. II, pp. 379–667.
5. *Pollutants from Air Traffic* (Results of Atmospheric Research in 1992–1997 years), ed. by U. Schumann (German Aerospace Center, Oberpfafenhofen, 1997), 290 pp.
6. O.B. Popovitcheva, A.M. Starik, and O.N. Favorskii, Izv. Ros. Akad. Nauk, Fiz. Atmos. Okeana **36**, No. 2, 163–176 (2000).
7. A.N. Kucherov, Atmos. Oceanic Opt. **13**, No. 5, 484–491 (2000).
8. L.E. Vasil'ev, S.I. Popov, and G.P. Svishchev, Tekhnika Vozd. Flota (TVF), Nos. 1–2, 14–17 (1994).
9. R.C. Miake-Lye, M. Martinez-Sanchez, R.C. Brown, and C.E. Kolb, J. of Aircraft **30**, No. 4, 469–479 (1993).
10. *Clouds and Cloudy Atmosphere: Handbook*, I.P. Mazin and A.Kh. Khrgian, eds. (Gidrometeoizdat, Leningrad, 1989), 647 pp.
11. A.N. Kucherov, Int. J. Heat and Mass Transfer **43**, No. 15, 2793–2806 (2000).
12. M.R. Poellot, W.P. Arnott, and J. Hallett, J. Geophys. Res. D **104**, No. 10, 12077–12084 (1999).
13. Y.T. Wang, Appl. Opt. **13**, No. 1, 56–62 (1974).
14. *Handbook of Lasers with Selected Data on Optical Technology*, R.J. Pressley, ed. (Chemical Rubber Co., Cleveland, 1971).
15. *TSAGI Reviews. No. 577. Flow Dynamics Problems in Laser Engineering,* M.N. Kogan, ed. (TSAGI Publishing Department, Moscow, 1980), 243 pp.
16. W.M. Irvine and J.B. Pollack, Icarus **8**, No. 2, 324–360 (1968).
17. J.W. Schaaf and D. Williams, J. Opt. Soc. Amer. **63**, No. 6, 726–732 (1973).
18. G.M. Hale and M.R. Querry, Appl. Opt. **12**, No. 3, 555–563 (1973).
19. M. Born and E. Volf, *Principles of Optics*, 4th edition (Pergamon Press, Oxford, 1968).
20. A.N. Kucherov, *Proc. of SOQUE. Int. Conf. LASERS'99*, V.J. and T.A. Corcoran, eds. (STS Press, USA, 2000), Vol. 22, pp. 143–150.
21. A.N. Kucherov, Proc. SPIE **5149**, 273–282 (2003).
22. Yu.A. Glagolev, *Handbook on Physical Properties of Atmosphere* (Gidrometeoizdat, Leningrad, 1970), 212 pp.
23. V.M. Nee and L.S.G. Kovasznay, The Physics of Fluids **12**, No. 3, 473–484 (1969).
24. A.H. Sekundov, Izv, Akad. Nauk SSSR, Mekh. Zhidkosti i Gasa, No. 5, 114–127 (1971).
25. A.V. Kashevarov, M.N. Kogan, A.N. Kucherov, and A.L. Stasenko, Atmos. Oceanic Opt. **10**, No. 12, 984–990 (1997).
26. V.A. Ruskol and U.G. Pirumov, Dokl. Akad. Nauk SSSR **246**, No. 2, 321–324 (1977).